Ultrasonic Study of First-Order and Second-Order Magnetoelastic Properties of Yttrium Iron Garnet*

D. E. EASTMAN†
Massachusetts Institute of Technology, Cambridge, Massachusetts
and
IBM Watson Research Center, Yorktown Heights, New York
(Received 3 March 1966)

First-order and second-order (in strain) magnetoelastic effects in yttrium iron garnet (YIG) have been studied using a pulsed ultrasonic technique and have been interpreted using finite-deformation magnetoelastic theory. Small-amplitude plane-wave modes in ⟨100⟩, ⟨110⟩, and ⟨111⟩ directions in uniformly magnetized, homogeneously deformed cubic single crystals have been analyzed including first-order and second-order magnetoelastic coupling. First-order and second-order magnetoelastic constants have been completely determined for YIG. The second-order "morphic" effect has been analyzed and completely evaluated for YIG in terms of 8 "morphic" constants. Experimental results are described which agree with finite-deformation magnetoelastic theory and disagree with small-strain theory.

I. INTRODUCTION

THE acoustic velocities of plane-wave-like modes in saturated ferromagnetic specimens depend on the magnetic-field strength and magnetization orientation.[1–3] Extensive measurements of these field-strength and magnetic-orientation dependencies have been made on single-crystal yttrium iron garnet (YIG) specimens and have been interpreted using phenomenological finite-deformation magnetoelastic (ME) theory. Finite-deformation ME theory is required to analyze second-order ME effects since the usual small-strain theory is valid only to first order in small quantities. For example, the symmetry of the second-order "morphic" effect, which results from magnetostrictive distortion and third-order (in displacement gradients) anelastic energy terms, is not identical to that of the intrinsic second-order ME interaction, as is incorrectly predicted using small-strain theory.

A pulsed ultrasonic technique capable of measuring small changes ($1:10^6$) in acoustic velocity has been used to measure the velocity dependence on magnetic field strength and magnetization orientation. Using these measurements, first-order ME constants and intrinsic second-order ME constants have been completely determined for YIG. Second-order morphic constants which characterize the "morphic" effect have also been completely determined. This work reports the first evaluation of intrinsic second-order ME constants and second-order "morphic" constants. Second-order ME constants are of interest in parametric magnon-phonon processes.[4–6]

In Sec. II, small-amplitude ME plane-wave propagation in a homogeneously saturated stress-free ferromagnetic medium is considered. The "morphic" effect is described and morphic constants are evaluated. Nondegenerate ME plane-wave modes in ⟨100⟩, ⟨110⟩, and ⟨111⟩ cubic crystal directions are determined. In Sec. III, the experimental technique is described and experimental results are presented and analyzed.

II. MAGNETOELASTIC PLANE-WAVE PROPAGATION

A. Basic Description

Small-amplitude plane-wave propagation in a magnetically saturated, homogeneously deformed single crystal is considered. A deformed medium must be considered in treating second-order (in strain) ME effects since ferro- and ferrimagnets possess a spontaneous magnetostrictive distortion.

It is convenient to describe every material particle by three positions: the *natural* reference position with coordinates $a_i=(a,b,c)$ in the undeformed reference state having density ρ_0, the *initial* deformed equilibrium position with coordinates $X_i=(X,Y,Z)$ at time t_0 in the initial state having density $\bar{\rho}$, and the present position with coordinates $x_i=(x,y,z)$ at time t in the present state having density ρ. All three positions are referred to the same Cartesian system. It is also convenient to introduce three displacement vectors:

$$u_i=x_i-X_i=(u,v,w)=\text{displacement from initial position to present position,} \quad (2.1a)$$

$$u_i'=X_i-a_i=(u',v',w')=\text{displacement from natural position to initial position,} \quad (2.1b)$$

* Based on a thesis submitted to the Department of Electrical Engineering, Massachusetts Institute of Technology, Cambridge, Massachusetts, in partial fulfillment of the Doctor of Philosophy degree, 1965. This work was sponsored in part by the Advanced Research Projects Agency under Contract SD-90. A brief summary of second-order magnetoelastic constants for YIG has been published [D. E. Eastman, J. Appl. Phys. 37, 996 (1966)].

† Present address: IBM Watson Research Center, Yorktown Heights, New York.

[1] W. P. Mason, Phys. Rev. 82, 715 (1951).

[2] G. A. Alers, J. R. Neighbors, and H. Sato, J. Phys. Chem. Solids 9, 21 (1958).

[3] J. Sakurai, J. Phys. Soc. Japan 19, 311 (1964).

[4] B. A. Auld, R. E. Tokheim, and D. K. Winslow, J. Appl. Phys. 34, 2281 (1963).

[5] F. R. Morganthaler, J. Appl. Phys. 34, 1287 (1963).

[6] B. A. Auld, Proc. IEEE 53, 1517 (1965).

$q_i = x_i - a_i = (q,r,s) =$ displacement from natural position to present position. (2.1c)

The deformation of the body is described in the material description by

$$x_i = x_i(a_i,t), \tag{2.2}$$

with

$$x_i(a_i,t_0) = X_i = X_i(a_i).$$

The magnetization per unit volume $\mathbf{M}$ is not conserved in a ferromagnet undergoing dilatational changes. Following Brown[7] and Tiersten,[8] it is assumed that the magnetic moment per unit mass, $\mathbf{m} = \mathbf{M}/\rho$, is conserved at fixed temperature.[9]

(2.3)

Equations of Motion

It is assumed that the state of the system is described by the temperature T or entropy S, deformation gradients $\partial x_i/\partial a_j$, magnetic moment per unit mass m_i, magnetic gradients $\partial m_i/\partial a_j$, applied magnetic field $\mathbf{H}_0$, and external surface force per unit area T_i. The general coupled isentropic equations of motion for the mechanical and magnetic systems have been derived[8,10,11]:

$$\rho \frac{d^2x_i}{dt^2} = \frac{\partial T_{ij}}{\partial x_j} + M_j \frac{\partial H_i}{\partial x_j}, \tag{2.4}$$

$$\frac{dm_i}{dt} = \gamma_0 \epsilon_{ijk} m_j H_k{}^e, \tag{2.5}$$

where

$$T_{ij} = \rho \frac{\partial x_j}{\partial a_p} \frac{\partial U}{\partial (\partial x_i/\partial a_p)} = \text{stress tensor}, \tag{2.6}$$

$$H_k{}^e = H_k - \frac{\partial U}{\partial m_k} + \frac{1}{\rho_0} \frac{\partial}{\partial a_j} \left(\rho_0 \frac{\partial U}{\partial (\partial m_k/\partial a_j)} \right) \tag{2.7}$$

$= $ effective magnetic field,

$U = U(S,\partial x_i/\partial a_j, m_i, \partial m_i/\partial a_j)$

$=$ local internal energy per unit mass,

$H_k = H_{0k} + H_k' =$ Maxwellian magnetic field,

$H_{0k} =$ applied magnetic field,

$H_k' =$ dipolar magnetic field,

$\gamma_0 = -\dfrac{g|e|}{2m_e c} =$ gyromagnetic ratio,[12]

$\epsilon_{ijk} =$ unit skew-symmetric tensor.

The stress tensor T_{ij} is not symmetric, owing to magnetic-body couples. The magnetic-body force term $M_j(\partial H_i/\partial x_j)$ in Eq. (2.4) is due to the interaction of the momentum M_j with the nonuniform field $\partial H_i/\partial x_j$. In Eq. (2.7), $\partial U/\partial m_k$ is an effective local field which describes ME and magnetocrystalline anisotropy interactions while the third right-hand-side term is the exchange interaction.

A more simple and convenient form of the mechanical equations of motion is obtained when all derivatives are transformed to natural-state variables. Using the identity[13]

$$\frac{\partial}{\partial x_k} \left(\frac{1}{J} \frac{\partial x_k}{\partial a_p} \right) = 0,$$

with

$$J = \frac{\rho_0}{\rho} = \frac{\partial(x_1,x_2,x_3)}{\partial(a_1,a_2,a_3)} = \text{Jacobian},$$

the mechanical equations of motion become

$$\rho_0 \frac{d^2x_i}{dt^2} = \frac{\partial P_{ik}}{\partial a_k} + \frac{\partial a_k}{\partial x_j} M_j \frac{\partial H_i}{\partial a_k}, \tag{2.8}$$

with

$$P_{ik} = \rho_0 \frac{\partial U}{\partial (\partial x_i/\partial a_k)}.$$

P_{ik} is the first Piola-Kirchoff stress tensor.[13]

The energy function $U(S,\partial x_i/\partial a_j, m_i, \partial m_i/\partial a_j)$ cannot be an arbitrary function of $\partial x_i/\partial a_j$, m_i, etc., because it must be invariant under all rigid motions of the deformed and magnetized body.[7,11,14] As shown by Tiersten,[8,11] this invariance requirement can be satisfied by using variables of the form[15]

$$U = U(S,\eta_{ij},\alpha_i{}^*,G_{ij}), \tag{2.9}$$

with

$$\eta_{ij} = \frac{1}{2} \left(\frac{\partial x_k}{\partial a_i} \frac{\partial x_k}{\partial a_j} - \delta_{ij} \right) = \text{strain tensor} \tag{2.10a}$$

$$= \frac{1}{2} \left(\frac{\partial q_i}{\partial a_j} + \frac{\partial q_j}{\partial a_i} + \frac{\partial q_k}{\partial a_i} \frac{\partial q_k}{\partial a_j} \right), \tag{2.10b}$$

$$\alpha_i{}^* = \frac{\partial x_k}{\partial a_i} \alpha_k, \tag{2.11}$$

$$G_{ij} = \frac{\partial \alpha_k}{\partial a_i} \frac{\partial \alpha_k}{\partial a_j}, \tag{2.12}$$

$$\alpha_i = \frac{m_i}{|\mathbf{m}|}. \tag{2.13}$$

[7] W. F. Brown, Jr., J. Appl. Phys. **37**, 994 (1965).
[8] H. F. Tiersten, J. Math. Phys. **6**, 779 (1965).
[9] This assumption is subject to scrutiny at high temperatures because of the thermodynamic definition of m_i.
[10] D. E. Eastman, Ph.D. thesis, Electrical Engineering Department, MIT, Cambridge, Massachusetts, 1965 (unpublished).
[11] H. F. Tiersten, J. Math. Phys. **5**, 1298 (1964).
[12] It is assumed in the following that the g factor is constant.
[13] *Physical Acoustics*, edited by W. P. Mason (Academic Press Inc., New York, 1964), Vol. I-A, p. 91-92.
[14] R. A. Toupin, J. Rational Mech. Anal. **5**, 849 (1956).
[15] The set of variables n_{ij}, $\alpha_i{}^*$, and G_{ij} in Eqs. (2.9)-(2.12) can be shown to be equivalent to Brown's (Ref. 7) E_{AB}, $\alpha_i{}^* = \alpha_k R_{ik}$, and $(\partial m_i/\partial X_c)(\partial m_i/\partial X_d)$. The $\alpha_i{}^*$'s in Eq. (2.11) are used in preference to Brown's $\alpha_i{}^*$'s as the latter are difficult to evaluate beyond first order in $\partial x_i/\partial a_j$.

Expanding U in the usual manner, one obtains

$$\begin{aligned}\rho_0 U=&\rho_0 U_0(S)\\&+g(\alpha_p{}^*,S)\\&+g_{ij}(\alpha_p{}^*,S)\eta_{ij}\\&+\frac{1}{2!}g_{ijkl}(\alpha_p{}^*,S)\eta_{ij}\eta_{kl}\\&+\frac{1}{3!}g_{ijklmn}(\alpha_p{}^*,S)\eta_{ij}\eta_{kl}\eta_{mn}\\&+\cdots\\&+\lambda_{ij}G_{ij}+\lambda_{ijkl}\eta_{ij}G_{kl}\\&+\cdots,\end{aligned}\tag{2.14}$$

with[16]

$$g(\alpha_p{}^*,S)=K_{ij}\alpha_i{}^*\alpha_j{}^*+\frac{1}{2!}K_{ijkl}\alpha_i{}^*\alpha_j{}^*\alpha_k{}^*\alpha_l{}^*+\cdots,\tag{2.15}$$

$$g_{ij}(\alpha_p{}^*,S)=\beta_{ij}+b_{ijkl}\alpha_k{}^*\alpha_l{}^*+\frac{1}{2!}b_{ijklmn}\alpha_k{}^*\alpha_l{}^*\alpha_m{}^*\alpha_n{}^*+\cdots,\tag{2.16}$$

$$g_{ijkl}(\alpha_p{}^*,S)=c_{ijkl}+B_{ijklmn}\alpha_m{}^*\alpha_n{}^*+\cdots,\tag{2.17}$$

$$g_{ijklmn}(\alpha_p{}^*,S)=C_{ijklmn}+\cdots,\tag{2.18}$$

$$K_{ij}=\frac{1}{2!}\left(\frac{\partial^2(\rho_0U)}{\partial\alpha_i{}^*\partial\alpha_j{}^*}\right)_{s,\eta,G}\Bigg|_{\alpha^*=\eta=G=0},$$

$$B_{ijklmn}=\frac{1}{2!}\left(\frac{\partial^4(\rho_0U)}{\partial\eta_{ij}\partial\eta_{kl}\partial\alpha_m{}^*\partial\alpha_n{}^*}\right)_{s,\eta,G}\Bigg|_{\alpha^*=\eta=G=0}.$$

In the spirit of Brugger,[17] thermodynamic definitions of the phenomenological constants $K_{ij}, \cdots, B_{ijklmn}, \cdots$ are used in Eqs. (2.14)–(2.18). These definitions minimize numerical complexity in actual calculations.

The various terms in Eqs. (2.14)–(2.18) are identified as follows: (1) ρ_0U_0 is the internal energy at zero α^*, η, G. (2) Equation (2.15) describes the magnetocrystalline anisotropy energy. It contains terms in $\partial x_i/\partial a_j$ due to the $\alpha_p{}^*$'s and, in principle, contributes to first-order and second-order ME effects. Usually $\alpha_p{}^*$ can be replaced by α_p, i.e., deformation effects can be ignored, because K_{ij}, K_{ijkl}, etc., are numerically very small compared to b_{ijkl}, B_{ijklmn}, etc. This is true for YIG and is expected to be true for nearly all ferro- and ferrimagnetic materials. (3) In Eq. (2.16), β_{ij} is related to entropy-dependent strains which arise when the initial-state entropy $\bar{S}$ differs from the natural-state reference entropy. In the analogous expansion of the Helmholtz free energy, the corresponding β_{ij} is related to thermal strains. The ME constants b_{ijkl} are the usual first-order magnetostrictive constants,[18] and the b_{ijklmn}'s are Becker-Döring constants. The latter are usually much smaller than the former. They are unimportant in the present study of ME wave propagation and are henceforth neglected. (4) In Eq. (2.17), the c_{ijkl}'s are the usual adiabatic elastic moduli. The B_{ijklmn}'s are second-order ME constants and are of principal interest in the present study. (5) In Eq. (2.18), the C_{ijklmn}'s are third-order elastic moduli. They are of interest because they are involved in the "morphic" effect. (6) In Eq. (2.14), the λ_{ij}'s and λ_{ijkl}'s are exchange and exchange-striction constants.

In Appendix I, the energy function U for the cubic point groups O, O_h, and T_d is given correct to second order in $\partial x_i/\partial a_j$ in ME energy terms and to third order in $\partial x_i/\partial a_j$ in mechanical-energy terms.

B. Morphic Effect

All ferromagnets with magnetostrictive coupling have a spontaneous magnetic-orientation-dependent distortion. In a uniformly magnetized stress-free cubic specimen this distortion is described to lowest order by the homogeneous static displacement gradients[19]:

$$\begin{aligned}&u_a'=h_1\bar{\alpha}_1{}^2, \quad v_c'=w_b'=h_2\bar{\alpha}_2\bar{\alpha}_3,\\&v_b'=h_1\bar{\alpha}_2{}^2, \quad u_c'=w_a'=h_2\bar{\alpha}_1\bar{\alpha}_3,\\&w_c'=h_1\bar{\alpha}_3{}^2, \quad u_b'=v_a'=h_2\bar{\alpha}_1\bar{\alpha}_2,\end{aligned}\tag{2.19}$$

with

$$h_1=-\frac{b_{11}}{c_{11}-c_2}, \quad h_2=-\frac{b_{44}}{2c_{44}},$$

$$u_a'\equiv\frac{\partial u'}{\partial a}=\frac{\partial u_1'}{\partial a_1}, \quad v_c'=\frac{\partial u_2'}{\partial a_3}, \text{ etc.}$$

The bars, $\bar{\alpha}_1$, etc., denote initial-state values.

Upon expanding the energy about the initial state and taking this deformation into account, both second-order and third-order (in strain) mechanical energies lead to energy terms of the form

$$C\frac{\partial u'}{\partial a}\left(\frac{\partial u}{\partial a}\right)^2\propto D(\bar{\alpha})^2\left(\frac{\partial u}{\partial a}\right)^2$$

with C and D being constants. This second-order ME effect, which is due to static magnetostrictive distortion and anelastic energy interactions, is called the "morphic" effect.[1] It is similar in form to the dominant

[16] Only terms having even powers in $\alpha_p{}^*$ are allowed because U must be invariant under time reversal.

[17] K. Brugger, Phys. Rev. 133, A1611 (1964).

[18] The b_{ijkl} reduce to b_1 and b_2, in the usual notation, for magnetically saturated cubic crystals.

[19] See W. F. Brown, *Micromagnetics*, (Interscience Publishers, Inc., New York, 1963), p. 124. The infinitesimal rotations $\frac{1}{2}(u_b'-v_a')$, etc., were set equal to zero in arriving at Eq. (2.19).

TABLE I. Morphic constants D_{ABC}.

Definition	Values ($\times 10^6$ erg/cc)
$D_{111}=h_1(3c_{11}-c_{12}+C_{111}-C_{112})$	$=20.4\ \pm 4.4$
$D_{123}=h_1(-c_{12}-c_{44}-C_{112}+C_{123})$	$=-11.3\ \pm 4.8$
$D_{144}=h_2(c_{12}-c_{44}+2C_{144})$	$=12.3\ \pm 2.6$
$D_{155}^{(1)}=h_2(c_{12}+3c_{44}+2C_{155})$	$=13.5\ \pm 1.5$
$D_{155}^{(2)}=h_2(c_{11}+c_{44}+2C_{155})$	$=13.1\ \pm 1.5$
$D_{441}^{(1)}=h_1(-2c_{44}+C_{144}-C_{155})$	$=-\ 0.3\ \pm 1.7$
$D_{441}^{(2)}=h_1(c_{11}-c_{12}-2c_{44})$	$=-\ 0.18\pm 0.01$
$D_{456}=h_2(2c_{44}+2C_{456})$	$=\ 2.2\ \pm 1.8$
with	
$h_1=\dfrac{-b_{11}}{c_{11}-c_{12}}$	$=-\ 2.24\pm 0.12\ (\times 10^{-6})$
$h_2=\dfrac{-b_{44}}{2c_{44}}$	$=-\ 4.61\pm 0.13$
Use c_{AB} and b_{AB} data[a]:	
$c_{11}=2.69\ (\times 10^{12}$ dyn/cm^2)	$b_{11}=(3.6\pm 0.2)\times 10^6$ dyn/cm^2
$c_{12}=1.077\ (\times 10^{12}$ dyn/cm^2)	$b_{44}=(7.2\pm 0.2)\times 10^6$ dyn/cm^2
$c_{44}=0.764\ (\times 10^{12}$ dyn/cm^2)	

[a] Elastic moduli c_{AB} data taken from Clark and Strakna (Ref. 22); b_{11} and b_{44} taken from Sec. III; C_{ABC} taken from Sec. II. All data are evaluated at room temperature.

$(\bar{\alpha})^2(\partial u/\partial a)^2$ terms in the intrinsic second-order ME energy.

The symmetry of the morphic effect on small-amplitude wave propagation is not identical to that of the linearized second-order ME energy because of contributions from $\frac{1}{2}c_{AB}\eta_A\eta_B$; if the symmetries were identical, one would need only to define new ME constants $B^{(\text{new})}=B+B^{(\text{mor.})}$ and proceed[20] [see Eqs. (A2)–(A4)]. This is due to the fact that third-order $\partial q/\partial a$ terms in $\frac{1}{2}c_{AB}\eta_A\eta_B$ cannot be rewritten in the form of a linearized third-order energy $\frac{1}{6}C'_{ABC}S_AS_BS_C$, where S_A is the infinitesimal strain,

$$S_A=(1-\tfrac{1}{2}\delta_{ij})\left(\frac{\partial q_i}{\partial a_j}+\frac{\partial q_j}{\partial a_i}\right),\quad ij\sim A,\quad A=1\cdots 6. \tag{2.20}$$

The morphic effect on small-amplitude wave propagation in cubic crystals is described by inserting the displacement gradients [Eq. (2.19)] in the general linearized equations obtained from the wave equations (2.4) or (2.8) and (2.5). This lengthy calculation is summarized in Eq. (A2) in Appendix I, where similarities and differences of the morphic and intrinsic second-order ME effects are clearly shown. It is observed that eight morphic constants D_{ABC} are needed to describe the morphic effect in cubic crystals (Table I). In the case of elastic isotropy ($c_{11}=c_{12}+2c_{44}$), $D_{155}^{(1)}=D_{155}^{(2)}$ and $D_{441}^{(2)}=0$ and the remaining six morphic constants have a one-to-one relation with the six intrinsic B_{ABC} constants, i.e., the symmetries of the morphic and intrinsic second-order ME effects on wave propagation are identical [see Eq. (A3)].

The morphic constants D_{ABC} can be determined if c_{AB},[21] b_{AB}, and C_{ABC} are known. The third-order elastic moduli C_{ABC} have been determined for YIG.[22] In units of 10^{12} dyn/cm^2 and at 28°C, they are (in the Brugger[17] notation):

$$C_{111}=-23.3\ \pm 0.8,\quad C_{144}=-1.48\pm 0.29,$$
$$C_{112}=-\ 7.14\pm 0.6,\quad C_{155}=-3.06\pm 0.14,$$
$$C_{123}=-\ 0.33\pm 1.3,\quad C_{456}=-0.97\pm 0.16.$$

Morphic constants for YIG are evaluated in Table I. A different set of constants results if the equations of motion are written in terms of initial state derivatives $\partial/\partial X_i$ instead of natural state derivatives $\partial/\partial a_i$.

The morphic effect is *static* in nature and consequently will not occur in high-frequency processes that use a time-varying magnetization $\alpha_i(t)$.[4,5] The general linearized equations (A2) and (A5) can be used to study such processes by simply setting the morphic constants equal to zero. A straightforward investigation of the morphic effect for time-varying $\alpha_i(t)$ indicates that it will retain its static character for frequencies well below the characteristic frequency $f_c\simeq V/2L$, where V is the acoustic velocity and L is a sample dimension. Near and above f_c, sample resonances are expected. These gradually diminish in amplitude with increasing frequency and damping and should have no practical effect for frequencies much higher than f_c.

C. Nondegenerate Plane-Wave Modes

The velocities and polarizations of small amplitude plane waves propagating in ⟨100⟩, ⟨110⟩, and ⟨111⟩ crystal directions are now considered. These modes have nearly pure shear or longitudinal elastic polarizations which permit individual modes to be excited using transducers. Modes are dominantly elastic in the low-frequency region of interest ($\omega\simeq 10^8$ rad/sec, $H_0=1$–10 kOe for experiments), with the ME interaction being a small perturbation, and will be characterized by their elastic polarizations.

The two shear modes in ⟨100⟩ and ⟨111⟩ propagation directions are degenerate in the unperturbed (pure elastic) approximation and consequently are sensitive to all perturbations, including small rod misalignment. While these nearly degenerate shear modes have interesting properties, such as magnetic-dependent acoustic Faraday rotation, and birefringence, they are difficult to use in determining ME constants because of this sensitivity to perturbations. Consequently, only the five nondegenerate modes in ⟨100⟩, ⟨110⟩, and ⟨111⟩ oriented rods are considered in this study.[23] These con-

[20] Earlier work on the morphic effect neglected these $\frac{1}{2}C_{ABn_An_B}$ contributions because of the use of small-strain theory (Refs. 1, 4).

[21] A. E. Clark and R. E. Strakna, J. Appl. Phys. **32**, 1172 (1961).

[22] D. E. Eastman, J. Appl. Phys. **37**, 2312 (1966). This work is also contained in Ref. 10.

[23] Rod misalignment effects on these nondegenerate modes add only a small *constant* perturbation to the velocity and do not affect the elastic polarizations.

TABLE II. Nondegenerate mode velocities in [001], [101], and [111] oriented rods.

Rod, orientation, mode	Natural velocity[a]
[001] rod, long. excit.	(1) $\rho_0 W^2 = c_{11} + [B_{111} + 5b_{11} + D_{111} + 4\pi M_s^2]\cos^2\theta - \left(\frac{2b_{11}}{M_s} - 4\pi M_s\right)^2 \sin^2\theta \cos^2\theta \chi_{11}$
[101] rod, long. excit.	(2) $\rho_0 W^2 = \frac{c_{11}+c_{12}+2c_{44}}{2} + \frac{1}{4}\{[-B_{111}+2B_{123}+4B_{441}-6b_{11}-4b_{44}-D_{11}+2D_{123}+4D_{441}^{(1)}-D_{441}^{(2)}]\sin^2\theta\sin^2\phi$ $+[4B_{155}+4b_{11}+6b_{44}+2D_{155}^{(1)}+2D_{155}^{(2)}](\cos^2\theta-\sin^2\theta\cos^2\phi)\} - \frac{1}{M_s^2}\{(b_{11}F_1+b_{44}F_2)^2\chi_{11}$ $+(b_{11}-b_{44})^2F_3^2\chi_{22}\} - \frac{1}{2}\{16\pi(b_{11}F_1+b_{44}F_2)\sin\theta\cos\theta\chi_{11} + 2[(4\pi M_s\sin\theta\cos\theta)^2\chi_{11} - 4\pi M_s^2\cos^2\theta)]\}$ with $F_1 = -\frac{\sin 2\theta}{2}\sin^2\phi$, $F_2 = -\frac{\sin 2\theta}{2}(1+\cos^2\phi)$, $F_3 = -\frac{\sin 2\phi}{2}\sin\theta$
[101] rod, shear excit., $\mathbf{u}\parallel\hat{b}'$([010])	(3) $\rho_0 W^2 = c_{44} + \frac{1}{2}\{(B_{456}+b_{44}+D_{456})(\cos^2\theta-\sin^2\theta\cos^2\phi) - (B_{441}+b_{11}-4b_{44}+D_{441}^{(1)}+D_{441}^{(2)})\sin^2\theta\sin^2\phi\}$ $-\left(\frac{b_{44}}{M_s}\right)^2[\cos^2 2\theta\sin^2\phi\chi_{11} + \cos^2\theta\cos^2\phi\chi_{22}]$
[101] rod, shear excit., $\mathbf{u}\parallel\hat{a}'$([10$\bar{1}$])	(4) $\rho_0 W^2 = \frac{c_{11}-c_{12}}{2} + \frac{1}{4}\{-[B_{111}+2B_{123}+6b_{11}+D_{111}+2D_{123}]\sin^2\theta\sin^2\phi + [2b_{44}-4b_{11}+2D_{155}^{(1)}-2D_{155}^{(2)}]$ $\times(\cos^2\theta-\sin^2\theta\cos^2\phi)\} - \left(\frac{b_{11}}{M_s}\right)^2(\cos^2 2\theta\cos^2\phi\chi_{11} + \cos^2\theta\sin^2\phi\chi_{22})$
[111] rod, long. excit.	(5) $\rho_0 W^2 = \frac{c_{11}+2c_{12}+4c_{44}}{3} + \frac{1}{3}[4B_{155}+2B_{144}+4B_{456}+4b_{11}+11b_{44}$ $+4\pi M_s^2+2D_{155}^{(1)}+2D_{155}^{(2)}+2D_{144}+4D_{456}]\cos^2\theta - \left(\frac{2b_{44}}{M_s}-4\pi M_s\right)^2\sin^2\theta\cos^2\theta\chi_{11}$
with	$\chi_{11} \simeq \frac{\omega_M}{4\pi(\omega_H+\omega_M\sin^2\theta)}$ $\omega_M = -\gamma_0 4\pi M_s$
	$\chi_{22} \simeq \frac{\omega_M}{4\pi\omega_H}$ $\omega_H = -\gamma_0(H_0+\bar{H}')$

[a] The constants D_{ABC} are summarized in Table I.

sist of longitudinal modes with ⟨100⟩, ⟨110⟩, and ⟨111⟩ propagation directions and two shear modes with a ⟨110⟩ propagation direction. All first-order and second-order ME constants can be evaluated using these five modes.

ME waves propagating in [001], [101], and [111] directions vary as

$$[001]: \quad u_i, \mu_i \sim \exp[i(Kc-\omega t)], \tag{2.21a}$$

$$[101]: \quad u_i, \mu_i \sim \exp\left[i\left(\frac{K}{\sqrt{2}}(a+c)-\omega t\right)\right], \tag{2.21b}$$

$$[111]: \quad u_i, \mu_i \sim \exp\left[i\left(\frac{K}{\sqrt{3}}(a+b+c)-\omega t\right)\right], \tag{2.21c}$$

with a, b, c = natural position coordinates, $\mu_i = \alpha_i - \bar{\alpha}_i$ = magnetic wave vector, $K = \omega/W$ = wave number, W = natural velocity. The natural velocity W is the wave speed referred to natural dimensions,

$$W = L_0/T_L, \tag{2.22}$$

where L_0 is the acoustic path length in the natural undeformed state and T_L is the acoustic transit time. Thurston and Brugger[24] give an excellent description of the natural velocity. It is advantageous to use the natural velocity instead of the actual velocity V,

$$V = W(L/L_0), \tag{2.23}$$

[24] R. N. Thurston and K. Brugger, Phys. Rev. 133, A1604 (1964).

where L is the initial-deformed-state path length, as length changes and propagation direction changes due to magnetostrictive distortion are then automatically taken into account.[24]

Nondegenerate small-amplitude wave velocities[25] and polarizations are obtained by substituting u_i and μ_i of Eq. (2.21) into Eqs. (A2) and (A5) and solving the resulting linearized equations. Results are summarized in Table II. The polar angles θ, ϕ denote the static magnetization direction in the laboratory coordinate system $(\hat{a}',\hat{b}',\hat{c}')$ defined in Fig. 1 (θ=polar angle measured from $\hat{c}'$, ϕ=aximuthal angle measured from $\hat{a}'$). The $\hat{c}'$ axis is taken parallel to the rod axes of rod specimens. Velocity expressions in Table II are independent of K and are valid in the low frequency region. The approximations $\omega \ll \omega_k$ and $\lambda K^2 \omega_M \ll \omega_H$ have been made, where ω_k is the spin-wave frequency.

More general dispersion relations valid in the crossover region can easily be obtained from those in Table II by substituting

$$W^2=(\omega/K)^2,$$

and

$$\chi_{22}=\frac{\omega_2\omega_M}{4\pi(\omega_k^2-\omega^2)},$$

$$\chi_{11}=\frac{\omega_1\omega_M}{4\pi(\omega_k^2-\omega^2)},$$

with

$$\omega_2=\omega_1+\omega_M\sin^2\theta,$$
$$\omega_{ex}=\lambda K^2\omega_M,$$
$$\omega_k^2=\omega_1\omega_2,$$
$$\omega_1=\omega_H+\omega_{ex},$$

and solving for ω versus K.

Various features of the modes in Table II are discussed in context with the experimental results. The magnetic body force [see Eq. (2.4)] affects only longitudinal modes to lowest order and results in b_{AB} appearing in the form $(b_{AB}-2\pi M_s^2)^2$ in longitudinal wave velocities, while appearing in the form $(b_{AB})^2$ in shear wave velocities.

[25] Equations (A2) and (A5) have been derived for a homogeneously saturated ferromagnet. Only ellipsoidal bodies can possess a uniform magnetization when placed in a finite uniform field and specimens of interest are cylindrical rods; however, the approximation of uniform $\mathbf{M}_s$ is a reasonable one in the high dc field region of interest $H_0 \gtrsim 2|\bar{H}'|$, where $\bar{H}'$ is the static demagnetizing field. The applicability in practice of the assumption of free mechanical boundary conditions is also subject to scrutiny, since nonspherical bodies oriented in a magnetic field experience a net torque exerted by the field which must be balanced by external surface forces from the specimen positioning apparatus. For YIG, a straightforward estimate of the average strain due to these forces yields $\partial u'/\partial a \simeq 10^{-8}$, which is two orders of magnitude smaller than the static strains due to magnetostriction.

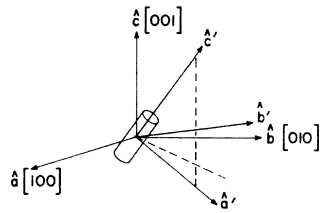

FIG. 1. Crystal coordinate system (a,b,c) and laboratory coordinate system (a',b',c'). The crystal directions of the laboratory system axes are as follows (rod axes along $\hat{c}'$):

Specimen orientation	$\hat{a}'$	$\hat{b}'$	$\hat{c}'$
[001]	[100]	[010]	[001]
[101]	[10$\bar{1}$]	[010]	[101]
[111]	[11$\bar{2}$]	[$\bar{1}$10]	[111]

III. EXPERIMENTAL METHODS AND RESULTS

A. Experimental Methods

First-order and second-order ME interactions have been studied by measuring the velocity dependence on field strength and magnetization orientation in magnetically saturated single YIG crystals. A pulsed ultrasonic system has been constructed[21] that is capable of measuring acoustic velocity changes of $1:10^6$ for 25–50 μsec acoustic delay times, which are readily available in high-Q YIG. In this system, which uses a phase-comparison technique, changes in the one-way acoustic transit time T_L are measured as changes in the carrier frequency f of the input pulse,

$$\Delta f/f=-\Delta T_L/T_L. \tag{3.1}$$

The carrier frequency f was adjustable in 20-cps steps over the 30±1.5-Mc/sec frequency range used.

The temperature was regulated to ±0.02°C near room temperature using a water jacket and circulator (Haake model Fe, Brinkmann Instruments, New York). Specimens were mounted in an orientation apparatus having two orthogonal rotational degrees of freedom with an angular resolution of $\pm\frac{1}{2}°$. The apparatus was positioned in a magnet supplying a 0–10 kOe field. X-cut and AC-cut quartz transducers (coaxial plated, $\frac{1}{8}$-in. diam) were used to generate longitudinal and linearly polarized shear excitations. Salol (phenyl salicylate) was used to bond transducers.

TABLE III. YIG specimens.[a]

Specimen number	Rod orientations	Dimensions (mm)
1	⟨100⟩	10.54×3.14 diam
2	⟨100⟩	8.47×3.63
3	⟨110⟩	10.47×3.20
4	⟨110⟩	13.63×3.125
5[b]	⟨111⟩	7.08×2.5

[a] Specimens 1 and 3 are from the Microwave Chemicals Laboratory, Inc., New York, New York; specimens 2 and 4 are from the Airtron Division of Litton Industries, Morris Plains, New Jersey and specimen 5 is from the IBM Watson Research Center, Yorktown Heights, New York.
[b] Specimen is approximately circular in cross section and has 1-μ finish.

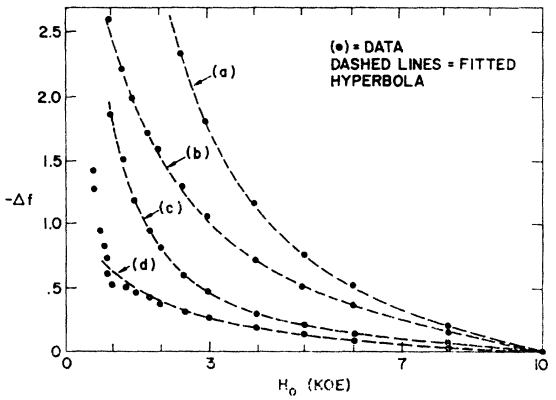

FIG. 2. Frequency change (kc/sec) versus field H_0 (kOe). [101] YIG rod (specimen No. 4). $T=28.8$°C. Shear excitation.

(a) $\mathbf{u}\|\hat{b}'([010])$, $\mathbf{M}_s\|\mathbf{K}(\theta=0)$, $f=29.76$ Mc/sec, measure $b_{44}=7.3\times10^6$ erg/cc.

(b) $\mathbf{u}\|\hat{b}'([010])$, $\mathbf{M}_s\|\mathbf{u}(\theta=\pi/2)$, $f=29.76$ Mc/sec, measure $b_{44}=7.2\times10^6$ erg/cc.

(c) $\mathbf{u}\|\hat{a}'([10\bar{1}])$, $\mathbf{M}_s\|\mathbf{K}(\theta=0)$, $f=30.15$ Mc/sec, measure $b_{11}=3.8\times10^6$ erg/cc.

(d) $\mathbf{u}\|\hat{a}'([10\bar{1}])$, $\mathbf{M}_s\|\mathbf{u}(\theta=\pi/2)$, $f=30.15$ Mc/sec, measure $b_{11}=3.6\times10^6$ erg/cc.

The cylindrical rod specimens which were used are described in Table III. The rod ends are optically polished and parallel and rod orientations are within ±2° of specified directions.

B. Experimental Results and Discussion

1. *First-Order ME Constants b_{11} and b_{44}*

Examination of mode velocities in Table II shows that perturbation terms which are an explicit function of the magnetic field (those containing χ_{11} or χ_{22}) involve b_{11} or b_{44}. These perturbations are due to small spin-wave admixtures in the ME modes. They are linear in χ_{11} or χ_{22} and result in velocity changes $\Delta V \propto (H_0+\text{const})^{-1}$ at fixed $\mathbf{M}_s$. This field dependence occurs because an increasing dc field lifts the spin wave manifold farther above the operating frequency, thereby pinning the magnetization more strongly and diminishing the spin wave admixture in the ME mode.

As seen from Table II, the shear modes (3) and (4) are most suitable for determining b_{11} and b_{44} as they have the strongest field dependence and involve b_{11} and b_{44} separately. The following four experiments were performed using sample No. 4:

Experiment

(a) [101] rod, $\mathbf{u}\|\hat{b}',\mathbf{M}_s\|\mathbf{K}$

$$\frac{\Delta W}{W}=-\frac{1}{2c_{44}}\left(\frac{b_{44}}{M_s}\right)^2\frac{M_s}{H_0+\bar{H}_{(a)}'}, \tag{3.2a}$$

(b) [101] rod, $\mathbf{u}\|\hat{b}',\mathbf{M}_s\|\mathbf{u}$

$$\frac{\Delta W}{W}=-\frac{1}{2c_{44}}\left(\frac{b_{44}}{M_s}\right)^2\frac{M_s}{H_0+\bar{H}_{(b)}'+4\pi M_s}, \tag{3.2b}$$

(c) [101] rod, $\mathbf{u}\|\hat{a}',\mathbf{M}_s\|\mathbf{K}$

$$\frac{\Delta W}{W}=-\frac{1}{(c_{11}-c_{12})}\left(\frac{b_{11}}{M_s}\right)^2\frac{M_s}{H_0+\bar{H}_{(a)}'}, \tag{3.2c}$$

(d) [101] rod, $\mathbf{u}\|\hat{a}',\mathbf{M}_s\|\mathbf{u}$

$$\frac{\Delta W}{W}=-\frac{1}{(c_{11}-c_{12})}\left(\frac{b_{11}}{M_s}\right)^2\frac{M_s}{H_0+\bar{H}_{(b)}'+4\pi M_s}, \tag{3.2d}$$

where $\bar{H}_{(a)}'$ and $\bar{H}_{(b)}'$ are average demagnetizing fields and ΔW is the natural velocity change due to the field-dependent ME interaction. Measured data (Δf versus H_0) is presented in Fig. 2. All frequency changes are measured relative to $\Delta f=0$ at $H_0=10$ kOe. Measured frequency changes and natural velocity changes are related, using Eqs. (2.22) and (3.1), according to

$$\Delta f/f=\Delta W/W. \tag{3.3}$$

It is seen in Fig. 2 that measured and predicted frequency responses, $\Delta f\propto(H_0+\text{const})^{-1}$, are in excellent agreement in the high-field region $H_0\gtrsim4\pi M_s=1760$ Oe. The dashed curves in Fig. 2 are calculated using the theoretical expression

$$-\Delta f(\text{cps})=C_1\left(\frac{1}{H_0+C_2}-\frac{1}{10+C_2}\right), \tag{3.4}$$

with H_0 in kOe and C_1, C_2 chosen for best fit to experimental data. The experimentally-determined constants C_1 are easily related to b_{11} and b_{44} using Eqs. (3.2), (3.3), and (3.4). Table IV summarizes experimental values of C_1 and C_2 and determined values of b_{11} and b_{44}. Excellent agreement between experiments (a) and (b) and between (c) and (d) is obtained. In experiments (a) and (c), z-directed ($\mathbf{M}_s\|\mathbf{K}$) spin waves are involved while x-y directed ($\mathbf{M}_s\perp\mathbf{K}$) spin waves are involved in experiments (b) and (d).

An alternative way to determine b_{11} and b_{44} from data in Fig. 2 is to use Eq. (3.2) and calculated average

TABLE IV. Determination of b_{11} and b_{44}.

Expt.	I. Curve fitting[a] C_1 (×10³ kOe/sec)	C_2 (kOe)	b_{11}, b_{44} (10⁶ erg/cc)	II. Prolate spheroid approx.[b] b_{11}, b_{44}	III. Uniform $\mathbf{M}_s$ approx.[c] b_{11}, b_{44}
(a)	7.5	−0.05	7.3	7.3	7.4
(b)	7.25	1.24	7.2	6.8	6.7
(c)	1.9	−0.05	3.8	3.7	3.8
(d)	1.8	1.24	3.6	3.3	3.3

[a] Values of c_{AB} in Table I and $4\pi M_s=1.76$ kOe were used. $\bar{H}_{(a)}'=-0.05$ kOe and $\bar{H}_{(b)}'=-0.52$ kOe. It is well known (Ref. 26) that b_{11} and b_{44} are positive.

[b] $\bar{H}_{(a)}'=-0.12$ kOe and $\bar{H}_{(b)}'=-0.82$ kOe.

[c] $\bar{H}_{(a)}'=-0.68$ kOe at $H_0=10$ kOe and $=-0.21$ kOe at $H_0=2$ kOe; $\bar{H}_{(b)}'=-0.79$ kOe at $H_0=10$ kOe and $=-0.78$ kOe at $H_0=2$ kOe.

demagnetizing fields $\bar{H}_{(a)}'$ and $\bar{H}_{(b)}'$ rather than curve-fitted values. This calculation has been performed for two approximations. In the first, the demagnetizing field of an inscribed prolate spheroid was used. In the second, assuming $\mathbf{M}_s$ is constant everywhere, the field $H'(z)$ along the rod axis due to surface poles was evaluated and the average group velocity $\bar{W}$ was calculated,

$$\bar{W}=W_0+\text{const}\langle H^{-1}\rangle_{\text{av}},$$

where W_0 is the uncoupled (infinite field) velocity and

$$\langle H^{-1}\rangle_{\text{av}}=\frac{1}{L_0}\int_0^{L_0}(H_0+H'(z)+4\pi M_s\sin^2\theta)^{-1}dz.$$

The average demagnetizing fields $\bar{H}'$ in Eq. (3.2) are then given in terms of $\langle H^{-1}\rangle_{\text{av}}$ by

$$\bar{H}'=\frac{1}{\langle H^{-1}\rangle_{\text{av}}}-H_0-4\pi M_s\sin^2\theta.$$

Results for these two approximate methods are summarized in Table IV. In the second method, data were evaluated using the field points $H_0=2$ and 10 kOe, since the effective demagnetizing fields $\bar{H}_{(a)}'$ and $\bar{H}_{(b)}'$ in $\langle H^{-1}\rangle_{\text{av}}$ are functions of H_0. Values for $\bar{H}_{(a)}'$ and $\bar{H}_{(b)}'$ in $\langle H^{-1}\rangle_{\text{av}}$ were calculated to approximately 1%. It is seen from Table IV that the agreement of curve-fitted and calculated values of b_{11} and b_{44} is fairly good even though curve-fitted and calculated internal fields differ considerably. The above experiments (a), (b), (c), and (d) were repeated using sample No. 3 and all determined values of b_{11} and b_{44} agreed to $\pm0.1\times10^6$ erg/cc with corresponding values in Table IV except experiment (c), for which the calculated value $b_{11}=4.0\times10^6$ erg/cc was obtained.

The ME constant b_{44} was also determined using a longitudinally excited [111] rod with θ fixed at 45° (see Table II). Using a prolate-spheroid demagnetizing field approximation, b_{44} was found to be 7.0×10^6 erg/cc.

Referring to Fig. 2, the curve marked (d) shows a distinct deviation from $\Delta f\propto(H_0+\text{const})^{-1}$ at low field strengths. This is a demagnetizing effect. The saturated-state internal demagnetizing field is about 900 Oe with $\mathbf{H}_0$ perpendicular to $\mathbf{K}$. This field strength corresponds quite closely to the point of abrupt change. Similar data on a transversely excited [001] rod showed an even more pronounced effect.

The shear velocities (3) and (4) in Table II indicate that no field dependence should be measured with $\mathbf{M}_s$ orthogonal to $\mathbf{K}$ and $\mathbf{u}$. This behavior was experimentally confirmed. With $\mathbf{u}$ parallel to $\hat{a}'$ or $\hat{b}'$, a frequency change less than 40 cps in 30 Mc/sec was obtained when H_0 was varied from 10 to 2 kOe. A comparably small frequency change was also measured for longitudinal modes in the [001], [101], and [111] directions with $\theta=0$ or $\pi/2$. This is expected from the formulas in Table II.

The constants b_{11} and b_{44} (b_1 and b_2 in the literature) have been determined at room temperature by other investigators using various techniques. Smith and Jones[26] used a ferromagnetic-resonance technique and determined $b_{11}=3.5\times10^6$ erg/cc and $b_{44}=7.0\times10^6$ erg/cc. Clark *et al.*[27] used a strain-gauge technique and determined $b_{11}=3.4\times10^6$ erg/cc and $b_{44}=6.6\times10^6$ erg/cc [their h_1 and h_2 are given by Eq. (2.22)]. Matthews and LeCraw[28] measured acoustic Faraday rotation in a ⟨100⟩ YIG rod and determined $b_{44}=7.4\times10^6$ erg/cc. Olson[29] measured the ME interaction effect on a microwave parallel pump threshold curve and determined $b_{44}=4.7\times10^6$ erg/cc. Comstock[30] has reviewed these various techniques.

2. *Second-Order ME Constants B_{ABC}*

Examination of mode velocities in Table II indicates somewhat complicated orientation-dependent perturbations involving second-order ME constants B_{ABC}, morphic constants D_{ABC}, and first-order ME constants b_{AB}. The angular dependence of these perturbations becomes simplified for orientation changes in the planes normal to $\hat{a}'$, $\hat{b}'$, and $\hat{c}'$. By measuring the velocity change as a function of orientation in these three planes for each of the five modes in Table II, the seven different linear equations involving the B_{ABC}'s listed in Table V can be evaluated. Maximum accuracy is obtained when all data are evaluated between the three $\hat{a}'$, $\hat{b}'$, and $\hat{c}'$ orientations, i.e., $(\theta,\phi)=(0,0)$, $(\pi/2,0)$ and $(\pi/2,\pi/2)$, using the largest possible dc field so as to minimize field-dependent perturbations.

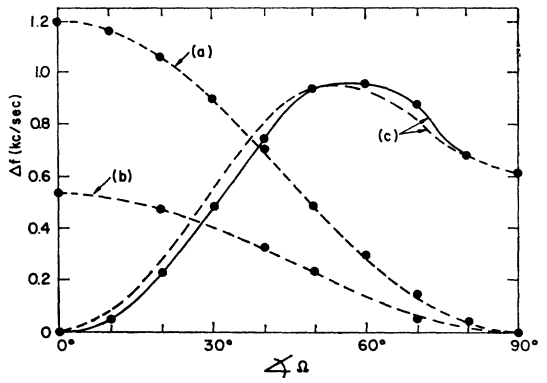

FIG. 3. Frequency change versus $\mathbf{M}_s$ orientation. [$\Omega=\theta$ for (a) and (c), $\Omega=\phi$ for (b).] Dashed lines are predicted curves using experimental constants. $H_0=10$ kOe. (a) [001] rod (specimen No. 1), long. excit., $f=30.60$ Mc/sec. (b) [101] rod (specimen No. 4), long. excit., $\theta=\pi/2$, vary ϕ, $f=29.22$ Mc/sec. (c) [101] rod (specimen No. 4), shear excit., $\mathbf{u}\|\hat{a}'([010])$, $\mathbf{M}_s\perp\hat{a}'(\phi=\pi/2)$, vary θ.

[26] A. B. Smith and R. V. Jones, J. Appl. Phys. 34, 1283 (1963).
[27] A. E. Clark, B. DeSavage, W. Coleman, and E. R. Callen, J. Appl. Phys. 34, 1296 (1963).
[28] H. Matthews and R. C. LeCraw, Phys. Rev. Letters 8, 397 (1962).
[29] F. A. Olson, J. Appl. Phys. 34, 1281 (1963).
[30] R. L. Comstock, Proc. IEEE 53, 1508 (1965).

TABLE V. Experiments and formulas for evaluating the magnetoelastic constants B_{ABC}.

Expt.	Rod orientation, mode	Orientation change[a] $(\theta,\phi)_1 \rightarrow (\theta,\phi)_2$	Formulas for B_{ABC}[b] $\left.\frac{\Delta f}{f}\right\|_2^2 = \left.\frac{\Delta f}{f}\right\|_1^2 - \left.\frac{\Delta f}{f}\right\|_1$
1.	[001] rod, long. excit.	$\left(\frac{\pi}{2},\phi\right) \rightarrow (0,\phi)$	(1) $B_{111}+5b_{11}+D_{111}=2c_{11}\left.\frac{\Delta f}{f}\right\|_1^2$
2.	[101] rod, shear excit. $\mathbf{u}\parallel\hat{a}'([10\bar{1}])$	$\left(\frac{\pi}{2},\frac{\pi}{2}\right) \rightarrow \left(\frac{\pi}{2},0\right)$	(2) $\frac{1}{4}[B_{111}+2B_{123}+2(5b_{11}-b_{11})+D_{111}+2D_{123}+2(D_{155}^{(2)}-D_{155}^{(1)})]-\left(\frac{b_{11}}{M_s}\right)^2\chi_{11}\Big\|_2 = 2\left(\frac{c_{11}-c_{12}}{2}\right)\left.\frac{\Delta f}{f}\right\|_1^2$
3.	[101] rod, shear excit. $\mathbf{u}\parallel\hat{b}'([010])$	$\left(\frac{\pi}{2},\frac{\pi}{2}\right) \rightarrow \left(\frac{\pi}{2},0\right)$	(3) $\frac{1}{2}[B_{441}-B_{456}+b_{11}-5b_{44}+D_{441}^{(1)}+D_{441}^{(2)}-D_{456}]+\left(\frac{b_{44}}{M_s}\right)^2\chi_{11}\Big\|_1 = 2c_{44}\left.\frac{\Delta f}{f}\right\|_1^2$
4.	[101] rod, shear excit. $\mathbf{u}\parallel\hat{b}'([010])$	$\left(\frac{\pi}{2},0\right) \rightarrow (0,\phi)$	(4) $B_{456}+b_{44}+D_{456}-\left(\frac{b_{44}}{M_s}\right)^2\chi_{11}\Big\|_2 = 2c_{44}\left.\frac{\Delta f}{f}\right\|_1^2$
5.	[101] rod, long. excit.	$\left(\frac{\pi}{2},0\right) \rightarrow (0,\phi)$	(5) $2B_{155}+2b_{11}+3b_{44}+D_{155}^{(1)}+D_{155}^{(2)}=2\left(\frac{c_{11}+c_{12}+2c_{44}}{2}\right)\left.\frac{\Delta f}{f}\right\|_1^2$
6.	[111] rod, long. excit.	$\left(\frac{\pi}{2},\phi\right) \rightarrow (0,\phi)$	(6) $\frac{1}{3}[4B_{155}+2B_{144}+4B_{456}+4b_{11}+11b_{44}+2D_{155}^{(1)}+2D_{155}^{(2)}+2D_{144}+4D_{456}] = 2\left(\frac{c_{11}+2c_{12}+4c_{44}}{3}\right)\left.\frac{\Delta f}{f}\right\|_1^2$
7.	[101] rod, long. excit.	$\left(\frac{\pi}{2},\frac{\pi}{2}\right) \rightarrow (0,\phi)$	(7) $\frac{1}{4}[B_{111}-2B_{123}+4B_{155}-4B_{441}+10(b_{11}+b_{44})+D_{111}-2D_{123}+2D_{155}^{(1)}+2D_{155}^{(2)}-4D_{441}^{(1)}] = 2\left(\frac{c_{11}+c_{12}+2c_{44}}{2}\right)\left.\frac{\Delta f}{f}\right\|_1^2$

[a] The subscripts 1 and 2 denote initial and final state.
[b] The D_{ABC}'s are defined in Table I. $4\pi M_s^2$ terms have been dropped in Eqs. (1), (5), and (6).

Three representative measurements of frequency change versus orientation are shown in Fig. 3. Curve (a) gives Δf versus θ for a longitudinally excited [001] oriented rod (sample No. 1). The dashed line is the function $\cos^2\theta$ predicted from formula (1) in Table II. (The $b_{11}^2\chi_{11}$ term is negligible at $H_0=10$ kOe.) The experimental resolution is $\Delta f/f \simeq 1.0\times10^{-6}$ and the total frequency change is $\Delta f/f = 40\times10^{-6}$.

Curve (b) in Fig. 3 gives frequency change versus orientation as $\mathbf{M}_s$ is rotated in the transverse plane ($\theta=\pi/2, \phi=0\rightarrow\pi/2$) of a [101] oriented rod. An isotropic material should show no frequency change under this rotation. Longitudinally excited [001] and [111] oriented rods exhibited no frequency change as $\mathbf{M}_s$ was rotated in the transverse plane; this is expected from formulas (1) and (5) in Table II.

Curve (c) in Fig. 3 exhibits more complicated behavior: $\Delta f(\theta)$ varies approximately as $\Delta f_1\cos^2\theta + \Delta f_2\sin^2 2\theta$, where Δf_1 and Δf_2 are constants. The $\sin^2 2\theta$ term is due to the field-dependent term $\propto\chi_{11}$ in formula (3) of Table II, which is still significant at $H_0=10$ kOe. (The difference in direction between $\mathbf{H}_0$ and $\mathbf{M}_s$ due to the demagnetizing field has been taken into account.) The disagreement between measured and predicted (dashed line) values is probably due to the variation of the demagnetizing field. An inscribed prolate ellipsoid demagnetizing factor was used in plotting the dashed line. Effects of such field-dependent terms on the determination of B_{ABC} constants are minimized by evaluating all data between $(\theta,\phi)=\hat{a}'$, $\hat{b}'$, and $\hat{c}'$ orientation directions.

Experimental frequency change versus orientation data were taken for all five modes in Table II using the samples listed in Table III. A summary appears in Table VI. Average data for specimens 1 and 2 and 3 and 4 are given in lines 1–10. The general angular dependence of Δf-versus-orientation curves predicted by formulas in Table II was observed in all experiments. The tolerances are estimated from the experimental frequency-change resolution and bracket experimental data on specimens 1 and 2 and 3 and 4. The sum of the three frequency changes corresponding to orientation

TABLE VI. Summary of frequency-change-versus-orientation data.

	Specimen	Rod orient.	Excit.	Orientation change $1 \rightarrow 2$	$10^6\left\|\frac{\Delta f}{f}\right\|_1^2 =$
1	1 and 2	[001]	long.	$\left(\frac{\pi}{2}, \phi\right) \rightarrow (0, \phi)$	39.3±1
2	3 and 4	[101]	long.	$\left(\frac{\pi}{2}, \frac{\pi}{2}\right) \rightarrow \left(\frac{\pi}{2}, 0\right)$	17.1±1
3	3 and 4	[101]	long.	$\left(\frac{\pi}{2}, 0\right) \rightarrow (0, \phi)$	− 3.8±1
4	3 and 4	[101]	long.	$(0, \phi) \rightarrow \left(\frac{\pi}{2}, \frac{\pi}{2}\right)$	−14.1±1
5	3 and 4	[101]	shear[a]	$\left(\frac{\pi}{2}, \frac{\pi}{2}\right) \rightarrow \left(\frac{\pi}{2}, 0\right)$	11.3±0.7
6	3 and 4	[101]	shear[a]	$\left(\frac{\pi}{2}, 0\right) \rightarrow (0, \phi)$	−36.0±1.7
7	3 and 4	[101]	shear[a]	$(0, \phi) \rightarrow \left(\frac{\pi}{2}, \frac{\pi}{2}\right)$	24.4±1
8	3 and 4	[101]	shear[b]	$\left(\frac{\pi}{2}, \frac{\pi}{2}\right) \rightarrow \left(\frac{\pi}{2}, 0\right)$	30.9±1
9	3 and 4	[101]	shear[b]	$\left(\frac{\pi}{2}, 0\right) \rightarrow (0, \phi)$	− 1.0±0.7
10	3 and 4	[101]	shear[b]	$(0, \phi) \rightarrow \left(\frac{\pi}{2}, \frac{\pi}{2}\right)$	−31.0±1
11	5	[111]	long.	$\left(\frac{\pi}{2}, \phi\right) \rightarrow (0, \phi)$	− 5.7±1.3

[a] $\mathbf{u} \| \hat{b}'$.
[b] $\mathbf{u} \| \hat{a}'$. $\left\|\frac{\Delta f}{f}\right|_1^2 \equiv \left\|\frac{\Delta f}{f}\right|_2 - \left\|\frac{\Delta f}{f}\right|_1$.
$T = 29 \pm 1$°C, $H_0 = 10$ kOe.

changes of (θ,ϕ) of $(\pi/2,\pi/2) \rightarrow (\pi/2,0)$, $(\pi/2,0) \rightarrow (0,\phi)$, and $(0,\phi) \rightarrow (\pi/2,\pi/2)$ provides a check on experimental accuracy.

ME constants B_{ABC} have been evaluated using the formulas in Table VI, and experimental data in Table VI, and c_{AB}, b_{AB}, and morphic constants in Table I. In units of 10^6 erg/cc, they are as follows:

B_{ABC} constants	Experiment 7 check
$B_{111} = 173 \pm 12$	
$B_{123} = 22 \pm 19$	$1/4(B_{111} - 2B_{123} + 4B_{155} - 4B_{441})$
$B_{144} = -5 \pm 41$	$= 19 \pm 33$ (calc)
$B_{155} = -37 \pm 5$	24 ± 12 (meas)
$B_{441} = -24 \pm 14$	
$B_{456} = -27 \pm 7$	

Experiments 1 through 6 have been used to evaluate the B_{ABC}'s and experiment 7 has been used as a consistency check.

Experimental error tolerances on the B_{ABC}'s are large, percentage-wise, but are relatively small energetically, as the B_{ABC}'s are small:

$$\tfrac{1}{2} c_{AB} |\eta_A \| \eta_B| \simeq 10^{12} |\eta_A|^2 \text{ erg/cc},$$
$$\tfrac{1}{2} B_{ABC} |\eta_A \| \eta_B \| \alpha_c^* \alpha_d^*| \simeq 10^7 |\eta_A|^2 \text{ erg/cc}.$$

Parametric spin-wave–phonon processes involving the second-order ME energy are expected to have high thresholds in YIG. According to Morgenthaler,[5] a spin-wave–phonon process can dominate the second-order spin-wave process if

$$\left|\frac{B_{111}}{c_{11}}\right| \quad \text{or} \quad \left|\frac{B_{441}}{c_{44}}\right| \gtrsim \frac{2}{Q}\left(\frac{4\pi M_s}{2\Delta H_k}\right)^{1/2},$$

with Q = acoustic quality factor,
ΔH_k = spin-wave linewidth.

For YIG, assuming $Q = 10^5$ and $\Delta H_k = 1$ Oe, this requires

$$\left|\frac{B_{111}}{c_{11}}\right| \quad \text{or} \quad \left|\frac{B_{441}}{c_{44}}\right| > 8 \times 10^{-4},$$

or

$$|B_{111}| \gtrsim 2000 \times 10^6 \text{ erg/cc},$$
$$|B_{441}| \gtrsim 500 \times 10^6 \text{ erg/cc}.$$

Measured values are $B_{111} = (173 \pm 12) \times 10^6$ erg/cc and $B_{441} = (-24 \pm 14) \times 10^6$ erg/cc. The threshold equations in Ref. 5 effectively neglect b_{AB} and $4\pi M_s^2$ terms compared with B_{ABC} because small-strain theory was used. This is a reasonable approximation in view of the small values of b_{AB} ($\simeq 5 \times 10^6$ erg/cc) compared with $B_{ABC} + b_{AB}$ values ($\simeq 2000$ or 500×10^6) that are required for interesting spin wave-phonon thresholds. Finite-deformation theory enables one to ascertain the validity of such approximations.

3. *Experimental Check on Finite-Deformation ME Theory*

This section describes an experiment that agrees with finite-deformation ME theory and disagrees with small-strain theory.

Referring to Eq. (4) in Table II, a [101] rod with a shear excitation $\mathbf{u} \| \hat{a}'([10\bar{1}])$ subjected to a 90° orientation change at constant H_0 in the $a'c'$ plane, i.e., $(\theta,\phi)_1 \rightarrow (\theta,\phi)_2$ is $(\pi/2,0) \rightarrow (0,\phi)$, will undergo a natural velocity change

$$\left.\frac{\Delta W}{W}\right|_1^2 = \frac{1}{(c_{11}-c_{12})}\left\{-2b_{11} + b_{44} + D_{155}^{(1)} - D_{155}^{(2)} - \left(\frac{b_{11}}{M_s}\right)^2 (\chi_{11}|_{\theta=0} - \chi_{11}|_{\theta=\pi/2})\right\}. \quad (3.5)$$

It is convenient to rewrite Eq. (3.5) in terms of the actual velocity $V=W(L/L_0)$ using the relation

$$\left|\frac{\Delta V}{V}\right|_1^2=\left|\frac{\Delta L}{L}\right|_1^2+\left|\frac{\Delta W}{W}\right|_1^2, \tag{3.6}$$

with the magnetostrictive length change determined as

$$\left|\frac{\Delta L}{L}\right|_1^2=h_2=-\frac{b_{44}}{2c_{44}}.$$

Upon substituting Eq. (3.6) in Eq. (3.5) and using the definitions of $D_{155}{}^{(1)}$ and $D_{155}{}^{(2)}$ in Eq. (A4), one obtains

$$\left|\frac{\Delta V}{V}\right|_1^2=\frac{1}{(c_{11}-c_{12})}\left\{-2b_{11}-\left(\frac{b_{11}}{M_s}\right)^2(\chi_{11}|_{\theta=0}-\chi_{11}|_{\theta=\pi/2})\right\}. \tag{3.7}$$

The term $-2b_{11}$ within the brackets is neglected in small-strain theory. It is due to the antisymmetric part of the stress tensor T_{ij} which originates from $\mathbf{M}\times\mathbf{H}$ body couples and which is accounted for by the use of the $\alpha_i{}^*$ rather than the direction cosines α_i in the ME energy.

The above experiment has been performed using specimens No. 3 and No. 4 with a 10-kOe dc field (see line 9 in Table VI). The measured velocity change is

$$\left|\frac{\Delta V}{V}\right|_1^2=\left|\frac{\Delta f}{f}\right|_1^2+\left|\frac{\Delta L}{L}\right|_1^2=(-5.6\pm0.8)\times10^{-6}, \tag{3.8}$$

with

$$\left|\frac{\Delta f}{f}\right|_1^2=(-1.0\pm0.7)\times10^{-6},$$

$$\left|\frac{\Delta L}{L}\right|_1^2=(-4.62\pm0.13)\times10^{-6}.$$

The calculated velocity change using finite deformation theory, i.e., Eq. (3.7), with b_{11} and b_{44} given in Table I, is

$$\left|\frac{\Delta V}{V}\right|_1^2=(-5.1\pm0.2)\times10^{-6}. \tag{3.9}$$

The calculated velocity change using small-strain theory [the $-2b_{11}$ term in Eq. (3.7) is set equal to zero] is

$$\left|\frac{\Delta V}{V}\right|_1^2=(-0.6\pm0.06)\times10^{-6}. \tag{3.10}$$

Comparison of Eq. (3.8) with Eq. (3.9) and Eq. (3.10) indicates good experimental agreement with finite deformation theory and an order of magnitude disagreement with small-strain theory. This experiment demonstrates the validity of finite deformation ME theory and illustrates the inexactness of small-strain theory in the treatment of second-order ME effects.

ACKNOWLEDGMENTS

The author is greatly indebted to Professor F. R. Morganthaler, who served as thesis advisor, for suggesting the problem and for many helpful and interesting discussions. Professor D. J. Epstein contributed many helpful discussions. R. A. Sparks of Airtron made available specimen No. 2.

APPENDIX: ENERGY FUNCTION U AND LINEARIZED EQUATIONS OF MOTION

A. Internal Energy U

The energy function U [Eqs. (2.14)–(2.18)] for the cubic point groups O, O_h, and T_d has the following form (Mason[1] and Hearman[31] have done work on the determination of independent coefficients b_{ijkl}, C_{ijklmn}, etc.):

$$\begin{aligned}\rho_0U=\rho_0U_0(S)&+\beta(\eta_1+\eta_2+\eta_3)+\frac{c_{11}}{2}(\eta_1^2+\eta_2^2+\eta_3^2)+c_{12}(\eta_1\eta_2+\eta_2\eta_3+\eta_3\eta_1)+\frac{c_{44}}{2}(\eta_4^2+\eta_5^2+\eta_6^2)\\&+\frac{C_{111}}{6}(\eta_1^3+\eta_2^3+\eta_3^3)+\frac{C_{112}}{2}(\eta_1^2(\eta_2+\eta_3)+\eta_2^2(\eta_3+\eta_1)+\eta_3^2(\eta_1+\eta_2))+C_{123}\eta_1\eta_2\eta_3+\frac{C_{144}}{2}(\eta_1\eta_4^2+\eta_2\eta_5^2+\eta_3\eta_6^2)\\&+\frac{C_{155}}{2}((\eta_1+\eta_2)\eta_6^2+(\eta_2+\eta_3)\eta_4^2+(\eta_3+\eta_1)\eta_5^2)+C_{456}\eta_4\eta_5\eta_6+b_{11}(\eta_1\alpha_1{}^{*2}+\eta_2\alpha_2{}^{*2}+\eta_3\alpha_3{}^{*2})\\&+b_{44}(\eta_4\alpha_2{}^*\alpha_3{}^*+\eta_5\alpha_3{}^*\alpha_1{}^*+\eta_6\alpha_1{}^*\alpha_2{}^*)+\frac{B_{111}}{2}(\eta_1^2\alpha_1{}^{*2}+\eta_2^2\alpha_2{}^{*2}+\eta_3^2\alpha_3{}^{*2})+B_{123}(\eta_1\eta_2\alpha_3{}^{*2}+\eta_2\eta_3\alpha_1{}^{*2}+\eta_3\eta_1\alpha_2{}^{*2})\\&+B_{144}(\eta_1\eta_4\alpha_2{}^*\alpha_3{}^*+\eta_2\eta_5\alpha_1{}^*\alpha_3{}^*+\eta_3\eta_6\alpha_1{}^*\alpha_2{}^*)+B_{155}((\eta_1+\eta_2)\eta_6\alpha_1{}^*\alpha_2{}^*+(\eta_2+\eta_3)\eta_4\alpha_2{}^*\alpha_3{}^*+(\eta_3+\eta_1)\eta_5\alpha_3{}^*\alpha_1{}^*))\\&+\frac{B_{441}}{2}(\eta_4^2\alpha_1{}^{*2}+\eta_5^2\alpha_2{}^{*2}+\eta_6^2\alpha_3{}^{*2})+B_{456}(\eta_4\eta_5\alpha_1{}^*\alpha_2{}^*+\eta_5\eta_6\alpha_2{}^*\alpha_3{}^*+\eta_6\eta_4\alpha_3{}^*\alpha_1{}^*)\\&+K_1(\alpha_1{}^{*2}\alpha_2{}^{*2}+\alpha_2{}^{*2}\alpha_3{}^{*2}+\alpha_3{}^{*2}\alpha_1{}^{*2})+\frac{4\pi\lambda}{2}(|\nabla_a m_1|^2+|\nabla_a m_2|^2+|\nabla_a m_3|^2),\end{aligned} \tag{A1}$$

[31] R. F. S. Hearman, Acta Cryst. 6, 331 (1953).

where

$$\eta_A=(2-\delta_{ij})\eta_{ij},\ ij\sim A,$$
$$K_1=\text{magnetocrystalline anisotropy constant},$$
$$\lambda=\text{exchange constant},$$
$$b_{AB}\sim b_{ijkl},\ \text{etc.}$$

The abbreviated notation of Brugger[17] has been used. The expression for the energy $\rho_0 U$ in Eq. (A1) is valid to second order in $\partial q_i/\partial a_j$ in ME terms and to third order in mechanical terms. The lowest order magnetocrystalline anisotropy energy is included in Eq. (A1) for generality. It is not considered in this paper. To second order in $\partial q_i/\partial a_j$, α_i^* may be replaced by α_i and η_A by S_A [Eq. (2.20)] in the second-order ME energy. In the first-order ME energy, the α_i^* lead to antisymmetric terms in the stress tensor.

B. Linearized Mechanical Equations of Motion

Mechanical equations of motion for a uniformly magnetized ferromagnet in a uniform external field free from applied forces are obtained using Eq. (2.8) and the energy function in Eq. (A1). The morphic effect is included by linearizing Eq. (2.8) about the initial deformed state having the displacement gradients of Eq. (2.19). Upon defining morphic constants D_{ABC} which are as analogous as possible to the intrinsic second-order constants B_{ABC}, the following equations of motion are obtained:

$$\rho_0\ddot{u}=c_{11}u_{aa}+c_{12}(v_{ab}+w_{ac})+c_{44}(u_{bb}+u_{cc}+v_{ab}+w_{ac})+2b_{11}\bar{\alpha}_1\frac{\partial\mu_1}{\partial a}+b_{44}\left(\bar{\alpha}_1\frac{\partial\mu_2}{\partial b}+\bar{\alpha}_2\frac{\partial\mu_1}{\partial b}+\bar{\alpha}_1\frac{\partial\mu_3}{\partial c}+\bar{\alpha}_3\frac{\partial\mu_1}{\partial c}\right)$$
$$+M_s\left(\bar{\alpha}_1\frac{\partial H_1}{\partial a}+\bar{\alpha}_2\frac{\partial H_1}{\partial b}+\bar{\alpha}_3\frac{\partial H_1}{\partial c}\right)+A_1\bar{\alpha}_1^2u_{aa}+A_2\bar{\alpha}_1\bar{\alpha}_2u_{ba}+A_2\bar{\alpha}_1\bar{\alpha}_3u_{ca}+(A_3\bar{\alpha}_3^2+A_4\bar{\alpha}_2^2)u_{bb}$$
$$+A_5\bar{\alpha}_2\bar{\alpha}_3u_{cb}+(A_3\bar{\alpha}_2^2+A_4\bar{\alpha}_3^2)u_{cc}+A_6\bar{\alpha}_1\bar{\alpha}_2(v_{aa}+v_{bb})+A_7\bar{\alpha}_3^2v_{ba}+A_8\bar{\alpha}_2\bar{\alpha}_3v_{ca}+A_8\bar{\alpha}_1\bar{\alpha}_3v_{cb}+A_9\bar{\alpha}_1\bar{\alpha}_2v_{cc}$$
$$+A_6\bar{\alpha}_1\bar{\alpha}_3(w_{aa}+w_{cc})+A_8\bar{\alpha}_2\bar{\alpha}_3w_{ba}+A_7\bar{\alpha}_2^2w_{ca}+A_9\bar{\alpha}_1\bar{\alpha}_3w_{bb}+A_8\bar{\alpha}_1\bar{\alpha}_2w_{cb},\quad\text{(A2)}$$

where

$$u_{ab}\equiv\partial^2u_1/\partial a_1\partial a_2\equiv\partial^2u/\partial a\partial b,\ \text{etc.},\ u_i=a_i-\bar{a}_i,$$
$$\bar{a}_i=\text{initial state value}.$$

The constants A_1–A_9 are defined in terms of b_{AB}, B_{ABC}, and D_{ABC} according to

$$\begin{aligned}
A_1&=B_{111}+5b_{11}+D_{111},\\
A_2&=2(B_{155}+2b_{44}+D_{155}^{(1)}),\\
A_3&=B_{441}-2b_{44}+D_{441}^{(1)},\\
A_4&=D_{441}^{(2)}+b_{11}-2b_{44},\\
A_5&=2(B_{456}+b_{44}+D_{456}),\\
A_6&=B_{155}+2b_{11}+b_{44}+D_{155}^{(2)},\\
A_7&=B_{123}+B_{441}-b_{44}+D_{123}+D_{441},\\
A_8&=B_{144}+B_{456}+b_{44}+D_{144}+D_{456},\\
A_9&=B_{456}+2b_{44}+D_{456}.
\end{aligned}\quad\text{(A3)}$$

The morphic constants D_{ABC} are defined in terms of c_{AB}, C_{ABC}, and b_{AB} according to

$$\begin{aligned}
D_{111}&=h_1(3c_{11}-c_{12}+C_{111}-C_{112}),\\
D_{123}&=h_1(-c_{12}-c_{44}-C_{112}+C_{123}),\\
D_{144}&=h_2(c_{12}-c_{44}+2C_{144}),\\
D_{155}^{(1)}&=h_2(c_{12}+3c_{44}+2C_{155}),\\
D_{155}^{(2)}&=h_2(c_{11}+c_{44}+2C_{155}),\\
D_{441}^{(1)}&=h_1(-2c_{44}+C_{144}-C_{155}),\\
D_{441}^{(2)}&=h_1(c_{11}-c_{12}-2c_{44}),\\
D_{456}&=h_2(2c_{44}+2C_{456}),
\end{aligned}\quad\text{(A4)}$$

with h_1 and h_2 defined in Eq. (2.19). Equations for $\rho_0\ddot{v}$ and $\rho_0\ddot{w}$ are obtained from Eq. (A2) by cyclic permutation of the components of a_i, u_i, μ_i, $\bar{\alpha}_i$, and H_i.

C. Linearized Magnetic Equations of Motion

Magnetic equations of motion are obtained for a uniformly magnetized ferromagnet in a uniform external field free from applied forces using Eq. (2.5). In the magnetostatic approximation ($\nabla\times\mathbf{H}=0$) and with u_i

and μ_i assumed to vary as

$$u_i, \mu_i \sim e^{i[KN_i a_i - \omega t]},$$

H_i^e is given to first order as

$$\begin{aligned} H_1^e = & H_{01} + \bar{H}_1' \\ & - \frac{1}{M_s}[2b_{11}\bar{\alpha}_1 u_a + b_{44}(\bar{\alpha}_2(u_b+v_a)+\bar{\alpha}_3(u_c+w_a)] \\ & - 4\pi M_s N_1[N_j(\mu_j - \bar{\alpha}_j(u_a+v_b+w_c)] \\ & + 4\pi\lambda\nabla_a^2 m_1, \end{aligned} \tag{A5}$$

with

N_i = unit vector in propagation direction,

H_{0i} = external field,

$\bar{H}_i'$ = static dipolar field.

Equations for H_2^e and H_3^e are obtained from Eq. (A5) by cyclic permutation. The third right-hand-side term in Eq. (A5) is the effective magnetoelastic coupling field linear in $\partial u_i/\partial a_j$. A similar term of the form $\mu_i(\partial u_j'/\partial a_k)$ has been dropped from Eq. (A5) because it is quite small. The fourth and fifth right-hand-side terms in Eq. (A5) are the dipolar (including the dilatational dipolar field) and exchange fields. Using Eq. (2.5), the linearized equations of motion are

$$\dot{\mu}_i = \gamma_0 \epsilon_{ijk}(\bar{\alpha}_j h_k^e + \mu_j \bar{H}_k^e), \tag{A6}$$

with h_k^e and $\bar{H}_k^e$ defined as the spatially varying and spatially nonvarying portions of H_k^e in Eq. (A5).

PHYSICAL REVIEW VOLUME 148, NUMBER 2 12 AUGUST 1966

Possible Experimental Test of the Band Theory of Magnetism

P. LEDERER AND D. L. MILLS*

Faculté des Sciences de Paris-Orsay, Service de Physique des Solides, Orsay, France

(Received 4 February 1966)

We suggest an experiment which may allow the band theory of ferromagnetism to be tested in a direct way. If a dc electric field is applied to a sample, the magnetic electrons will drift. The frequency of a spin wave of given wave vector, when viewed in the laboratory frame, will suffer a Doppler shift when compared with the case when the electric field is zero. This Doppler shift, although small, is considerably larger for the band model than the electric field dependence of the spin-wave dispersion relation for a localized spin model. We discuss the possibility of detecting the Doppler shift by measuring the phase velocity of a coupled spin–transverse-phonon wave. Similar measurements have been performed on insulators doped with paramagnetic impurities. In these measurements, high precision has been obtained by employing an interference technique which allows a null experiment to be performed.

I. INTRODUCTION

VARIOUS models have been proposed to describe the magnetic properties of transition metals. While these models assume very different mechanisms are responsible for the magnetically ordered state, they nonetheless predict elementary excitation spectra and thermodynamic properties which are qualitatively similar. As a consequence, it is difficult to decide from experimental measurements which of the models is most suited to describe the magnetism of the transition metals.

Historically, the first approach to the problem was by Heisenberg,[1] who employed a model of localized spins, each coupled to its nearest-neighbor spins by means of the exchange interaction which results from the overlap of atomic orbitals. If the exchange integral has the appropriate sign, the ground state of the system is ferromagnetic. The elementary excitations of the system are spin waves,[2] and one finds that as the temperature is increased from zero, the change in magnetization varies as $T^{3/2}$, in agreement with experimental observations. This model has been studied extensively. A number of other magnetic properties of transition metals, such as the variation of the magnetic susceptibility with temperature just above the Curie point,[3] and the magnetic critical scattering observed in neutron diffraction experiments[4] may be accounted for with this theory. In the Heisenberg model, the interaction between the localized spins is short-ranged, since the wave function of a given spin overlaps appreciably only with its nearest neighbors. The conduction electrons (s electrons) play no role, as far as the magnetic properties of the system are concerned.

* National Science Foundation Postdoctoral Fellow.

[1] We refer the reader to the review article by J. H. Van Vleck, Rev. Mod. Phys. **17**, 27 (1945).

[2] F. Bloch, Z. Physik **61**, 206 (1930).

[3] See for instance, M. E. Fisher, in *Proceedings of the International Conference on Magnetism, Nottingham, 1964* (Institute of Physics and the Physical Society, London 1965), p. 79.

[4] R. J. Elliott and W. Marshall, Rev. Mod. Phys. **30**, 75 (1958).